Measurements of the Gain, Time Resolution, and Spatial Resolution of a 20×20 cm^2 MCP-based Picosecond Photo-Detector

Bernhard Adams[a], Andrey Elagin[b,*], Henry Frisch[b], Razib Obaid[b,1], Eric Oberla[b], Alexander Vostrikov[b], Robert Wagner[a], Matthew Wetstein[b]

[a]*Argonne National Laboratory, 9700 S. Cass Ave., Lemont, IL 60439, U.S.A*
[b]*Enrico Fermi Institute, University of Chicago, 5640 S. Ellis Ave., Chicago, IL 60637, U.S.A*

Abstract

Microchannel plates (MCPs) allow for micron-level spatial imaging and picosecond-level time resolution, making them a good choice for the next generation of photo-detectors aiming for precision time-of-flight measurements. The Large-Area Picosecond Photo-Detector Collaboration (LAPPD) is currently developing a 20×20 cm^2, thin, planar, glass-body detector with two MCPs in chevron geometry with 8° bias angle. The modular design of the strip-line anode allows covering large areas while keeping the number of electronics channels low. We have built a complete detector system approximating the final detector design. We have measured gain up to 2×10^7, time-of-flight resolution up to 35 ps, differential time resolution of ∼6 ps, and spatial resolution better than 1 mm.

Keywords: MCP, TOF,

1. Introduction

Microchannel plates [1] are capable of micron-level spatial resolution[2] and picosecond-level time resolution [3, 4, 5]. The Large-Area Picosecond Photo-Detector Collaboration (LAPPD) is currently developing a 20×20 cm^2, thin, planar, glass-body detector based on MCPs [6]. To achieve fast timing with large-area coverage, the LAPPD collaboration invested effort into the development of the MCPs, photocathode, hermetic packaging, and integrated readout system. Atomic layer deposition (ALD) is employed to produce low cost MCPs [7, 8]. The signal readout is provided by an economical RF strip-line anode [9] and PSEC-4 waveform digitizing ASIC [10]. Applications for large-area fast detectors include collider experiments, neutrino physics, X-ray physics and Positron-Emission Tomography.

2. LAPPD Detector and Test Setups

Figure 1 shows a schematic view of the LAPPD detector. The sealed vacuum package consist of a pair of MCPs in a chevron geometry. Three grid spacers provide gaps between the photocathode and top MCP, between MCPs, and between the bottom MCP and anode.

In such a detector photo-electrons ejected from a photocathode are accelerated in a potential gap before they reach a stack of two MCPs. These electrons are amplified by secondary electron emission within pores of the MCPs, which are held at an electric field of ∼1 kV/mm. The pores of the two plates are oriented at a bias angle of 8° to prevent drift of positive ions to the photocathode and to ensure a well-defined first strike of the incoming electrons. The avalanche of secondary electrons is collected at the anode circuit.

The detector components are made of widely available float glass. The anode is made by silk-screening of the silver strips onto glass. The anode strip-lines share a copper ground plate located at the bottom of the detector. This produces a flat panel detector with a thickness of less than 15 mm.

No pins are required to provide high voltage on the MCPs and in the gaps. There is a single high voltage cable connected to the photocathode window. High voltage distribution between the internal components is controlled by the resistance of the MCPs and the grid spacers which have a resistive ALD layer. A DC current going through the whole vertical stack is grounded at each anode strip-line through 10 kΩ resistors. An equivalent electrical circuit for high voltage distribution in the LAPPD detector is shown in Fig. 2.

We have assembled a facility for testing of the MCP-based detector systems and their individual components at the Advanced Photon Source (APS) at Argonne National Laboratory (ANL). MCPs are tested in a device-level configuration using a pulsed laser capable of sub-picosecond pulses. Details on this testing facility can be found in [12]. Here we provide only a brief description of two setups capable of testing large area (20×20 cm^2) MCPs.

Figure 3 shows the large testing vacuum chamber, where MCPs sit in a glass tray designed to the specification of the LAPPD sealed-tube. Since the plates are in vacuum, this setup is free from the constraint of sealing the tube, allowing for independent high voltage control of the individual components

[*]*Corresponding author.* E-mail address: elagin@hep.uchicago.edu
[1]Present address: Illinois Institute of Technology, Department of Physics, 3101 South Dearborn St., Chicago, IL 60616

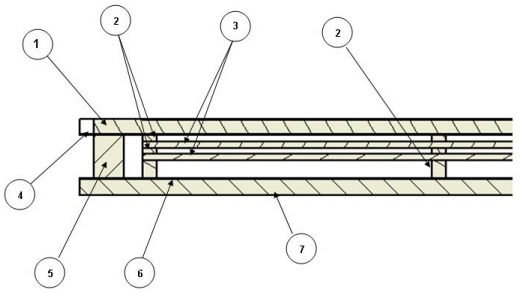

Figure 1: Schematic view of an LAPPD MCP-based detector.

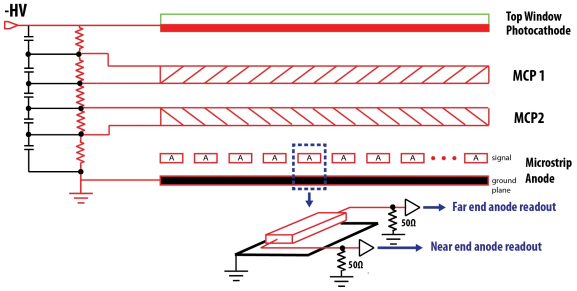

Figure 2: The circuit diagram for the high voltage distribution.

and various spacing between photocathode, MCPs, and anode. An aluminum photocathode is used in this setup to allow for assembly in air. The low quantum efficiency of the photocathode is compensated for by the high intensity of the laser pulses. The signals from the anode strip-lines are brought out of the chamber to a multi-GHz-bandwidth oscilloscope through vacuum feedthroughs with SMA cables.

Figure 4 shows the Demountable assembly, a prototype configuration to test and validate the final LAPPD detector design. The differences between the Demountable and LAPPD are: 1) the tube stays under active pumping rather than being hermetically sealed with getter material inside; 2) the seal between the top window and the tube body is achieved by mechanical compression on an O-ring rather than an indium seal; and 3) the photocathode is a thin Aluminum layer on a quartz window rather than bialkali on float glass.

The modular design of the LAPPD detector is demonstrated in Fig. 4, where one active Demountable detector shares a readout with three passive 30-strip anodes connected serially. The 90-cm long anode reliably provides an analog bandwidth of 400 MHz and 50 Ω impedance. Details on the anode design and characteristics can be found in [9].

The signal from the Demountable is read out either using a multi-GHz bandwidth oscilloscope in which the signal is sent through high frequency RF cables, or using a fully integrated LAPPD-designed front-end electronics system based on the PSEC-4 chip [10]. The PSEC-4 ASIC is a 1.5 GHz, 15 Gs/s chip with 6 channels. Two analog cards with five PSEC-4 chips

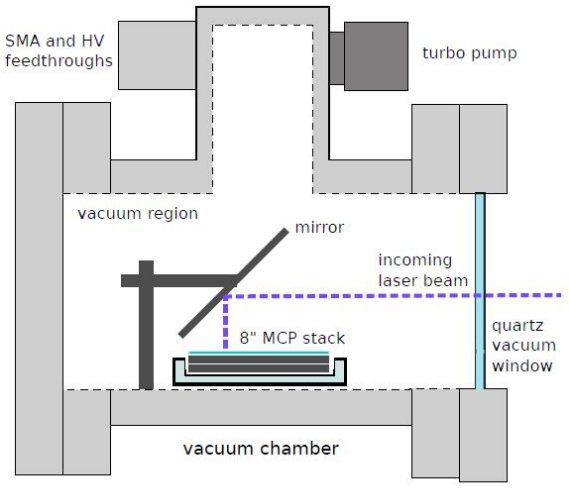

Figure 3: A schematic view of the vacuum chamber for testing 8" MCPs. The laser beam enters through the quartz window and is reflected onto the stack of aluminum photocathode, two MCPs in chevron geometry and strip-line anode.

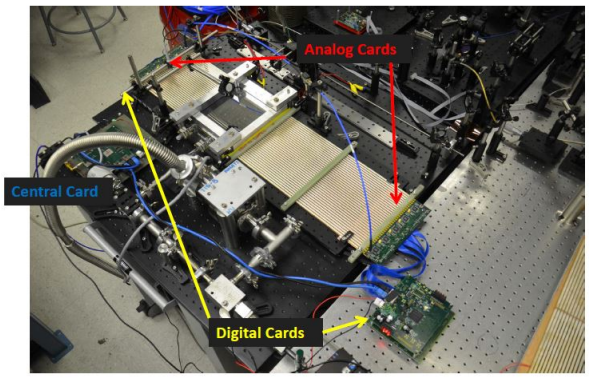

Figure 4: Photo of the Demountable setup demonstrating modular design. One active resealable detector module shares a ~90 cm long delay-line anode with three, currently inactive, modules.

are connected directly to the anode at each side of the detector. Each analog card is connected to a digital card which independently determine the times and charges of the pulses at each side. The central card uses this information to reconstruct the position, arrival time and total charge. The position along the strip-lines is reconstructed based on the time difference at the two ends. The position in the direction perpendicular to the strip-lines is reconstructed based on the signal centroid.

3. Results

In the testing program we use a Ti:Sapph laser with a rise time smaller than 50 fs and a full width of the order 100–200 fs [12]. Triggering on such short pulses allows for precise measurements of the time resolution of MCP-based detector systems. For the present work we measure the arrival time of the MCP signal at 25% threshold of the total signal amplitude. We measure the time-of-flight resolution defined as the

RMS of the time of the MCP signal with respect to a fast photodiode trigger, which precisely registers the time of each laser pulse.

We also measure the differential time resolution defined as the RMS of the time difference in the signal arrival at the opposite ends of the anode strip-line. The differential time resolution directly translates into the spatial resolution in the direction parallel to the anode strip-line. The correspondence between the position resolution (δX) and differential time resolution (δT) is given by $\delta X = \frac{1}{2} V \delta T$, where V is the signal propagation speed along the anode strip-line. The latter can be determined by moving the laser beam along the strip-line and measuring the change in the differential timing.

3.1. Results from the vacuum chamber setup

A typical pulse-height distribution for a pair of ALD-MCPs in the vacuum chamber is shown in Fig. 5. Based on the calibration of the laser system, as discussed in [12], we estimate that operation of this setup was close to single photo-electron operation. From this estimate the gain for a pair of plates to be 2×10^7.

Figure 6 shows typical pulses and the difference in the time-of-arrival of the signal to the opposite ends of the anode strip-line, measured as a function of the laser beam position along the strip-line. The slope of 11.75 mm/ps corresponds to a signal propagation velocity of 0.57 c, which is in agreement with an independent measurement of this parameter with network analysis of the anodes [9].

While we benefit a lot from the use of our short-pulse powerful laser, it creates experimental challenges for time resolution measurements in our setup. Pulses from the MCPs overlap with RF noise introduced by the Pockels cells in the laser. The structure and the level of the noise can be seen on the pulse frames shown in Fig. 6. Figure 7 shows the differential time resolution as a function of noise-to-signal ratio at a fixed position of the laser beam.

A simulation of the differential time resolution was performed in which varying amplitude MCP pulses were generated and co-added with broadband white noise. The linear dependence of this simulation matches the observed data. The offset between data and simulation is consistent with a non-zero size of the laser beam spot. For pulses with high gain and, therefore, low noise-to-signal ratio we observe a differential time resolution of ~6 ps which translates into spatial resolution of ~0.5 mm.

3.2. Results from the Demountable

One of the main goals of the Demountable setup is to test the readout designed for large-area coverage. Here we demonstrate the performance of a 90-cm long anode with electronics based on the PSEC-4 chip. In the current setup, shown in Fig. 4, only one of the 4 anodes has an active detector with MCPs. However the signal is read out only after it propagates through two more anodes on one side and one additional anode on the other side. Such four-anode structures can be assembled in a "Super Module", a large area 3×4 LAPPD detector system designed

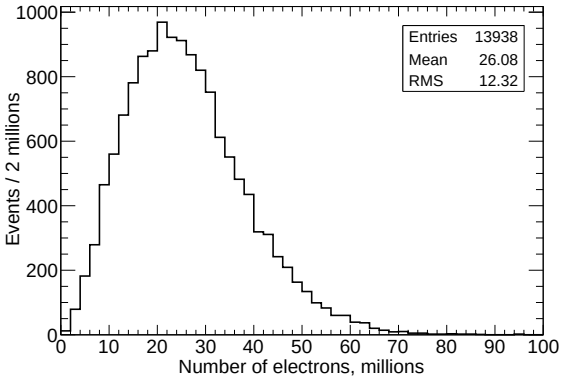

Figure 5: MCP pulse-height distribution measured in the large vacuum chamber setup.

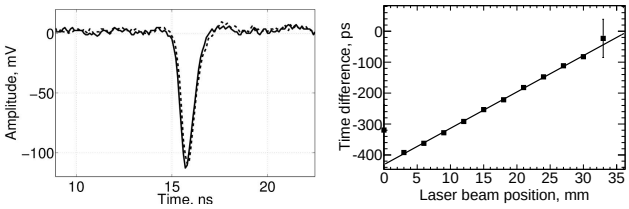

Figure 6: Left: an example of MCPs pulses at the opposite sides of the anode strip-line in the large vacuum chamber setup. Near side (solid line) and far side (dotted line). Right: difference in the time of arrival of the signal to the opposite ends of the anode strip-line as a function of laser beam position along the strip-line, data (points) compared to the linear fit (line).

to reduce number of channels by sharing the same delay line pattern of several MCPs.

Typical pulses[2] seen at the opposite sides of the anode strip-lines are shown on the left-hand plot of Fig. 8. The difference in the signal arrival time as a function of the laser beam position with respect to the anode is shown on the right-hand plot of Fig. 8. From the slope parameter of the linear fit we measure a signal propagation velocity of 0.55 c.

We tested the Demountable as a time-of-flight system by trig-

[2]The optical pass from the laser to the photocathode has less attenuation in the Demountable setup than in the large vacuum chamber setup which results in a higher number of photo-electrons per laser pulse.

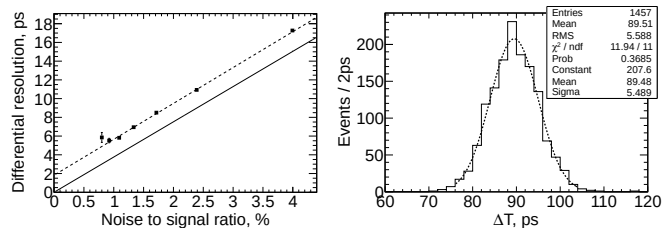

Figure 7: Left: differential time resolution evaluated at a fixed laser position along the strip-line, shown as a function of noise-to-signal ratio. The offset between a linear fit of the data (dotted line) and the simulation (solid line) is consistent with the size of the laser beam spot. Right: differential time for pulses with noise-to-signal ratio smaller than 1.2%, data (solid line) compared to the gaussian fit (dotted line).

gering on the laser pulse and measuring the time spread in the arrival time of the MCP signal. Figure 9 shows the time spread measured with two different readout systems. We observe a ~35 ps time-of-flight resolution with our 3.5 GHz, 10 Gs/s oscilloscope and ~80 ps resolution with LAPPD electronics based on PSEC-4 chip. In the data presented here, no dedicated calibration of the LAPPD electronics has been done to optimize timing performance. Improvements in the timing performance will be discussed in the forthcoming publications.

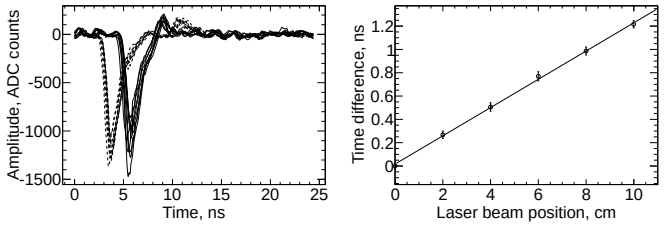

Figure 8: Left: an example of MCPs pulses at the opposite sides of the anode strip-line in the Demountable. Near side (solid lines) and far side (dotted lines). Right: difference in the time of arrival of the signal to the opposite ends of the anode strip-line as a function of laser beam position along the strip-line, data (points) compared to the linear fit (line).

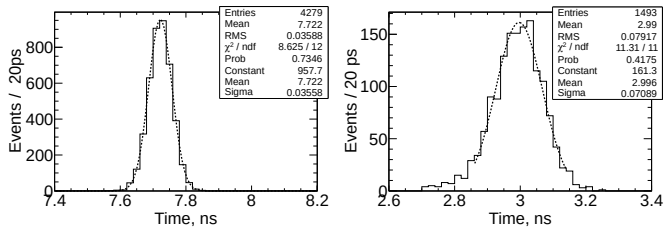

Figure 9: Time-of-flight resolution of the Demountable setup measured with 3.5 GHz, 10 Gs/s oscilloscope (left) and with LAPPD electronics based on the custom front-end PSEC-4 chip. Data (solid lines) is compared to the gaussian fit (dotted lines).

4. Conclusion

We have presented measurements of the gain and timing characteristics of large-area MCPs functionalized with ALD process. Our test setups approximate the design of the large area photodector system which includes a strip-line anode and fully integrated electronics. We demonstrate that such detector systems are capable of $\sim 2\times10^7$ gains and a time-of-flight resolution up to 35 ps. In the regime of low noise-to-signal ratio, we measure ~6 ps differential time resolution between the opposite ends of the anode strip-line, which corresponds to a spatial resolution of ~0.5 mm.

5. Acknowledgments

This work would not have been possible without the dedicated effort of Joe Gregar of the Glass Shop at ANL, Richard Northrop and Robert Metz of the University of Chicago Engeneering Center, Mary Heintz and Mark Zaskowski of the University of Chicago Electronics and Development Group, and Harold Gibson and Haidan Wen of the Advanced Photon Source at ANL. We would like to thank Jeffrey Elam and Anil Mane of the Energy Systmes Division at ANL for providing the ALD functionalized MCPs used in these measurements. We are greatful to Gary Drake of the High Energy Physics Division at ANL for help with the electronic noise. We thank Dean Walters of the Nuclear Engineering Division at ANL for help with vacuum packaging and Jeffrey Williams of the High Energy Physics Division at ANL for help with MCPs flow between different facilities at ANL. We thank Jason McPhate and Oswald Siegmund for advice and encouragement.

The work at ANL was supported by the U.S. Department of Energy Office of Science, Office of Basic Energy Science and Office of High Energy Physics under contract DE-AC02-06CH11357 and at the University of Chicago by the National Science Foundation under grant PHY-1066014.

References

[1] J. L. Wiza, *Microchannel plate detectors*, Nucl. Instrum. Methods 162 (1979) 587-601.

[2] A.S. Tremsin and O.H.W. Siegmund, *Charge cloud asymmetry in detectors with biased MCPs* Proceedings SPIE3, vol. 4497, San Diego, California (2001).

[3] T. Credo, H. Frisch, H. Sanders, R. Schroll, and F. Tang; "Time-of-Flight Systems with Picosecond Resolution", Proceedings of the IEEE, Rome, Italy, Oct. 2004; Nuclear Science Symposium Conference Record, 2004 IEEE, Volume 1.

[4] J. Milnes, J. Howorth, *Picosecond Time Response of Microchannel Plate PMT Detectors* Proc. SPIE vol 5580 (2005) pp 730-740.

[5] At the 2005 UC Workshop on Fast Timing (http://hep.uchicago.edu/workshops/2005-picosecond/) T. Ohshima reported on results from an MCP with a Cherenkov-radiation induced signal. The Nagoya group has now achieved a 4.7 psec resolution: K. Inami, N. Kishimoto, Y. Enari, M. Nagamine, and T. Ohshima , *A 5-ps TOF-counter with an MCP-PMT*; Nucl.Instrum.Meth.A560:303-308,2006.

[6] The LAPPD Collaboration, http://psec.uchicago.edu

[7] J. W. Elam, G. Xiong, C. Y. Han, HH Want, J. P. Birrell, U. Welp, J. N. Hyrn, M. J. Pellin, T. F. Baumann, J. F. Poco, and J. H. Satcher, Atomic Layer *Deposition for the Conformal Coating of Nanoporous Materials*, Journal of Nanomaterials, 2006, p. 1-5.

[8] N. Sullivan, P. de Rouffignac, D. Beaulieu, A. Tremsin, K. Saadatmand, D. Gorelikov, H. Klotzsch, K. Stenton, S. Bachman, R. Toomey, *Novel microchannel plate device fabricated with atomic layer deposition*, in: Proceedings of the Ninth International Conference on Atomic Layer Deposition, Monterey, CA, July 2009.

[9] H. Grabas, H. Frisch, E. Oberla, J.-F. Genat, R. Northrop, D. McGinnis, B. Adams, M. Wetstein, R. Obaid, F. Tang, *RF Strip-Line Anodes for Psec Large-Area MCP-based Photodetectors*, Nucl. Instrum. Methods A711 (2013) 124-131.

[10] E. Oberla, H. Grabas, J.-F. Genata, H. Frisch, K. Nishimura, G. Varner, *A 15 GSa/s, 1.5 GHz Bandwidth Waveform Digitizing ASIC for fast Detector Readout*, submitted to Nucl. Instrum. Methods A.

[11] B. Adams, A. Elagin, J. Elam, H. Frisch, J.-F. Genat, J. Gregar, A. Mane, R. Northrop, E. Oberla, A. Vostrikov, R. Wagner, M. Wetstein, *An Internal ALD-Based High Voltage Divider and Signal Circuit for MCP-based Photodetectors*, in preparation.

[12] B. Adams, M. Chollet., A. Elagin., E. Oberla, A. Vostrikov, M. Wetstein, R.Obaid, P.Webster, *A Test-Facility for Large-area Microchannel Plate Detector Assemblies Using a Pulsed sub-Picosecond Laser*, submitted to Review of Scientific Instruments.